

# Incommensurate Magnetic Fluctuations in $\text{YBa}_2\text{Cu}_3\text{O}_{6.6}$

Pengcheng Dai,<sup>1</sup> H. A. Mook,<sup>1</sup> and F. Doğan<sup>2</sup>

<sup>1</sup>*Oak Ridge National Laboratory, Oak Ridge, Tennessee 37831-6393*

<sup>2</sup>*Department of Materials Science and Engineering*

*University of Washington, Seattle, Washington 98195*

(August 10, 2018)

## Abstract

We use inelastic neutron scattering to demonstrate that at low temperatures, the low frequency magnetic fluctuations in  $\text{YBa}_2\text{Cu}_3\text{O}_{6.6}$  ( $T_c = 62.7$  K) are incommensurate, being found at positions displaced by  $\pm\delta$  ( $0.057 \pm 0.006$  r.l.u.) along the  $[\pi, \pi]$  direction from the wave vector  $(\pi, \pi)$  associated with the antiferromagnetic order of the parent insulator,  $\text{YBa}_2\text{Cu}_3\text{O}_6$ . The dynamical susceptibility  $\chi''(\mathbf{q}, \omega)$  at the incommensurate positions increases on cooling below  $T_c$ , accompanied by a suppression of magnetic fluctuations at the commensurate points.

PACS numbers: 74.72.Bk, 61.12.Ex

Knowledge of the spin dynamical properties of the cuprates are crucial to the understanding of high-temperature ( $T_c$ ) superconductivity. An important issue is the symmetry of the imaginary part of the dynamical susceptibility,  $\chi''(\mathbf{q}, \omega)$ , probed directly by neutron scattering. Over the past several years, intensive experimental work on the single layer  $\text{La}_{2-x}\text{Sr}_x\text{CuO}_4$  (214) [1,2] and the bilayer  $\text{YBa}_2\text{Cu}_3\text{O}_{7-x}$  [(123) $\text{O}_{7-x}$ ] [3–9] cuprates has yielded valuable information concerning the magnetic response in the normal and superconducting states. For the 214 family, magnetic fluctuations were found at incommensurate positions from the antiferromagnetic ordering position  $(\pi, \pi)$  [1]. For (123) $\text{O}_{7-x}$ , the situation is more subtle. While Rossat-Mignod and coworkers only detected magnetic fluctuations at the commensurate position  $(\pi, \pi)$  [3], Tranquada *et al.* [4] noticed that the wave vector dependence of  $\chi''(\mathbf{q}, \omega)$  in a (123) $\text{O}_{6.6}$  ( $T_c = 53$  K) crystal was better described by a pair of identical Gaussians displaced symmetrically from the  $(\pi, \pi)$  point, suggesting possible incommensurate fluctuations. In a subsequent experiment, Sternlieb *et al.* [4] have suggested that the wave vector dependence of the susceptibility is independent of energy for all energies between 2 mV and 40 meV. Although the nontrivial wave vector dependence behavior was again observed,  $\chi''(\mathbf{q}, \omega)$  was not found to be different below and above  $T_c$ . No firm conclusions about the commensurability and symmetry of  $\chi''(\mathbf{q}, \omega)$  were reached [4].

In this Letter, we present inelastic neutron scattering data which resolves the issue of commensuration in (123) $\text{O}_{6.6}$ . We show that the magnetic response is complex with incommensurate fluctuations for energies below the commensurate resonance [8] at low temperatures. The low frequency spin fluctuations change from commensurate to incommensurate on cooling with the incommensuration first appearing at temperatures somewhat above  $T_c$ . Lowering the temperature suppresses the spin fluctuations at the commensurate points, accompanied by an increase in the susceptibility at the incommensurate positions.

Our results shed light on several long standing theoretical predictions. If the (123) $\text{O}_{7-x}$  system is indeed a  $d$ -wave superconductor,  $d$ -wave gap nodes could yield incommensurate peaks below  $T_c$  [10]. In this scenario, the scattering of (123) $\text{O}_{6.6}$  is expected to be commensurate in the normal state and incommensurate in the superconducting state [11]. No neutron

scattering experiment, until now, has observed this behavior. Second, even though the differences in the commensurability in  $(123)\text{O}_{7-x}$  and 214 can be explained from the Fermi surface differences between the two compounds [12], such models have not been entirely reconciled with the nuclear magnetic resonance (NMR) measurements [13,14]. The reconciliation of the neutron and NMR results requires detailed information about the structure of  $\chi''(\mathbf{q}, \omega)$  [15]. The third theoretical conjecture stems from recent neutron scattering experiments of Tranquada *et al.* [16] which suggest that the incommensuration in superconducting 214 may be associated with a spatial segregation of charge or charge density wave correlations [17]. If the idea of dynamical microphase separation in the  $\text{CuO}_2$  plane asserted by Emery and Kivelson [18] is relevant for the high- $T_c$  superconductivity, one would expect incommensurate spin fluctuations in other cuprate superconductors like  $\text{Bi}_2\text{Sr}_2\text{CaCu}_2\text{O}_{8-x}$  (2212) and  $(123)\text{O}_{7-x}$ . Indeed, recent neutron scattering experiments by Mook and Chakoumakos [19] show that the spin fluctuations in 2212 are also incommensurate. Thus, incommensurability may be a common feature for all cuprate superconductors.

The neutron scattering measurements were made at the High-Flux Isotope Reactor at Oak Ridge National Laboratory using the HB-1 and HB-3 triple-axis spectrometers. The fabrication and characteristics of our single-crystal sample of  $(123)\text{O}_{6.6}$  (weight 25.59 grams and  $T_c = 62.7$  K) were described in detail previously [8]. The major difficulty in studying spin fluctuations in the  $(123)\text{O}_{7-x}$  system is to separate the magnetic scattering from (single- and multi-) phonon and other spurious processes. While multi-phonon scattering usually has a simple wave vector dependence and spurious events such as accidental Bragg scattering can be identified by checking the desired inelastic scan in the two-axis mode [4], two approaches can be used to separate magnetic from single-phonon scattering. The first approach is to perform neutron polarization analysis [20] which, in principle, allows an unambiguous separation of magnetic and nuclear scattering. This method has been successfully employed to identify the magnetic origin of resonance peaks for ideally [5] and underdoped [8,9]  $(123)\text{O}_{7-x}$ . However, this advantage comes at a considerable cost in intensity which makes the technique impractical for observing small magnetic signals. The second approach

is to utilize the differences in the temperature and wave vector dependence of the phonon and magnetic scattering cross sections. While phonon scattering gains intensity on warming due to the thermal population factor, the magnetic signal usually becomes weaker because it spreads throughout the energy and momentum space at high temperatures. Thus, in an unpolarized neutron measurement the net intensity gain above the multi-phonon background on cooling at appropriate wave vectors is likely to be magnetic in origin.

Figure 1(a) depicts the reciprocal space probed in the experiment with  $\mathbf{a}^*$  ( $=1/a$ ),  $\mathbf{b}^*$  ( $=1/b$ ) directions shown in the square lattice notation. The momentum transfers  $(q_x, q_y, q_z)$  in units of  $\text{\AA}^{-1}$  are at positions  $(H, K, L) = (q_x a/2\pi, q_y b/2\pi, q_z c/2\pi)$  reciprocal lattice units (r.l.u.). We first describe measurements made in the  $(H, H, L)$  zone. Our search for the magnetic fluctuations was done with the filter integration technique [21] first developed to study the chain fluctuations in  $(123)\text{O}_{6.93}$ . This technique is excellent for isolating scattering from lower dimensional objects and relies on integrating the energy along wave vector direction  $[0, 0, L]$  perpendicular to the scan direction  $[H, H, 0]$ . To estimate the energy integration range of the technique, we note that the scattered intensity for acoustic modulations in  $(123)\text{O}_{7-x}$  is proportional to the in-plane susceptibility  $\chi''(q_x, q_y, \omega)$  [4,22]

$$I(\mathbf{q}, \omega) \propto \frac{k_f}{k_i} |f_{\text{Cu}}(\mathbf{q})|^2 \sin^2\left(\frac{1}{2}\Delta z q_z\right) [n(\omega) + 1] \chi''(q_x, q_y, \omega),$$

where  $k_i$  and  $k_f$  are the initial and final neutron wave numbers,  $f_{\text{Cu}}(\mathbf{q})$  is the  $\text{Cu}^{2+}$  magnetic form factor,  $\Delta z$  ( $=3.342 \text{ \AA}$ ) the separation of the  $\text{CuO}_2$  bilayers,  $\mathbf{q}$  the total momentum transfer ( $|\mathbf{q}|^2 = q_x^2 + q_y^2 + q_z^2$ ), and  $[n(\omega) + 1]$  the Bose population factor. The solid line in Fig. 1(b) shows the calculated  $I(\mathbf{q}, \omega)$  at  $(\pi, \pi)$  as a function of energy transfer (along  $q_z$ ) assuming  $\chi''(q_x, q_y, \omega) = F(q_x, q_y)\chi''(\omega) \propto \omega F(q_x, q_y)$  [23]. Although there are two broad peaks in the figure, the observed intensity will mostly stem from fluctuations around the lower energy one ( $10 < \Delta E < 30 \text{ meV}$ ) because of the decreased resolution volume at large energy transfers. Since room temperature triple-axis measurements show no detectable magnetic peaks at  $(\pi, \pi)$  below 40 meV (see Figs. 2 and 3), we have used the integrated scan at 295 K as the background and assumed subsequent net intensity gains above the multi-phonon

background at lower temperatures are magnetic in origin. Figure 1(c) shows the result at different temperatures. At 200 K, the magnetic fluctuations are broadly peaked at  $(\pi, \pi)$ . On cooling to 150 K and 100 K, the peak narrows in width and grows in intensity but is still well described by a single Gaussian centered at  $(\pi, \pi)$ . At 65 K, the data show a flattish top similar to previous observations [4]. Although detailed analysis suggests that the profile is better described by a pair of peaks (Lorentzian or Lorentzian-squared line-shape) than a single Gaussian, the most drastic change in the profile comes in the low temperature superconducting state. Rather than the expected single peak, two peaks at positions displaced by  $\pm\delta$  ( $0.057 \pm 0.006$  r.l.u.) from  $H = 0.5$  are observed, accompanied by a drop in the spin fluctuations at the commensurate position. The observation of sharp incommensurate peaks with the filter integration technique suggests that the incommensuration must be weakly energy dependent in the integration range.

Although the integration technique is excellent in finding small peaks from the scattering of lower dimensional objects, it is important to confirm the result with conventional triple-axis measurements and to determine the symmetry of the incommensuration. For this purpose, we have realigned the sample in the  $(H, 3H, L)$  zone. If the 15 K profile in Fig. 1(c) stems from an incommensurate structure with peaks at  $(0.5 \pm \delta, 0.5 \pm \delta)$  [see Fig. 1(a)], scans along the  $[H, 3H]$  direction are expected to peak at  $H = 0.477$  and  $0.523$  r.l.u. for  $\delta = 0.057$ . On the other hand, if the underlying symmetry is identical to that of 214 [rotated  $45^\circ$  from Fig. 1(a)], the incommensuration in a  $[H, 3H]$  scan should occur at  $H = 0.466$  and  $0.534$  r.l.u. Figure 2 summarizes the result at 24 meV [24]. The scattering at room temperature shows no well defined broad peak around  $(\pi, \pi)$ , but at 70 K a two peak structure emerges. On cooling below  $T_c$ , the spectrum rearranges itself with a suppression of fluctuations at commensurate point accompanied by an increase in intensity at incommensurate positions. The wave vectors of the peaks in the  $[H, 3H]$  scan are consistent with incommensuration at  $(0.5 \pm \delta, 0.5 \pm \delta)$ . It may also be possible to interpret the data with other structures, however, we will assume the symmetry of Fig. 1(a) until more precise measurements are made.

In previous work, superconductivity was found to induce a strong enhancement in the  $\chi''(\mathbf{q}, \omega)$  at  $(\pi, \pi)$  for ideally [3,5–7] and underdoped [8,9]  $(123)\text{O}_{7-x}$  at the resonance positions. Although the intensity gain of the resonance below  $T_c$  is accompanied by a suppression of fluctuations at frequencies above it for the underdoped compounds [8,9], no constant-energy scan data are available at energies above the resonance. In light of the present result at 24 meV for the  $(123)\text{O}_{6.6}$  sample which has a resonance at 34 meV [8], it is important to collect data at these frequencies. Thus, we undertook additional measurements with improved resolution (collimation of  $50''$ - $40''$ - $40''$ - $120''$ ) in the hope of resolving possible incommensuration at high energies. Figures 3(a) and (b) suggest that the fluctuations at the resonance energy are commensurate above and below  $T_c$  with no appreciable change in width. For an energy above the resonance (42 meV), the scan is featureless at room temperature but shows a well defined peak centered at  $(\pi, \pi)$  at 75 K. Although superconductivity suppresses the magnetic fluctuations [see inset of Fig. 3(d)], the wave vector dependence of the line-shape cannot be conclusively determined due to the poor instrumental resolution at this energy. Unfortunately, further reduction in resolution volume is impractical due to a concomitant drop in the scattering intensities.

Since the earlier polarized work [8] has shown that for  $(123)\text{O}_{6.6}$  the 34 meV resonance is the dominant feature of  $\chi''(\mathbf{q}, \omega)$  at  $(\pi, \pi)$  in the low temperature superconducting state, it is important to compare the newly observed incommensurate peaks to the intensity gain of the resonance. Figure 4 shows the difference spectra between 15 K and 75 K at frequencies below and above the resonance. In the energy and temperature range of interest (15 K to 75 K), the phonon scattering changes negligibly and the Bose population factor  $[n(\omega) + 1]$  modifies the scattered intensity at high temperatures by only 3% at 24 meV and less at higher energies. Therefore, the difference spectra in the figure can be simply regarded as changes in the dynamical susceptibility. Inspection of Figs. 4(a) and (b) reveals that the susceptibility at the incommensurate positions increases on cooling from the normal to the superconducting state, accompanied by a suppression of fluctuations at the commensurate point. Comparison of Fig. 4(c) to Figs. 4(a) and (b) indicates that the net gain in intensity at

the incommensurate positions below  $T_c$  is much less than that of the resonance. For an energy transfer of 42 meV, the intensity drop appears uniform throughout the measured profile, however, instrumental resolution may mask any possible incommensurate features. Figure 4(e) plots a summary of the triple-axis measurement in superconducting state. Although there are only two constant-energy scans for frequencies below the resonance, these data nevertheless confirm the result of the integrated technique.

In conclusion, we have found that the low frequency magnetic fluctuations in a  $(123)\text{O}_{6.6}$  sample are incommensurate at low temperatures with incommensuration first appearing at temperatures above  $T_c$ . The dynamic susceptibility at incommensurate positions increases on cooling below  $T_c$ , accompanied by a suppression of magnetic fluctuations at the commensurate point.

We thank G. Aeppli, V. J. Emery, K. Levin, and D. Pines for helpful discussions. We have also benefited from fruitful interactions with J. A. Fernandez-Baca, R. M. Moon, S. E. Nagler, and D. A. Tennant. This research was supported by the US DOE under Contract No. DE-AC05-96OR22464 with Lockheed Martin Energy Research Corp.

## REFERENCES

- [1] S-W. Cheong *et al.*, Phys. Rev. Lett. **67**, 1791 (1991); T. E. Mason *et al.*, *ibid.* **68**, 1414 (1992); *ibid.* **71**, 919 (1993); *ibid.* **77**, 1604 (1996); S. M. Hayden *et al.*, *ibid.* **76**, 1344 (1996).
- [2] T. R. Thurston *et al.*, Phys. Rev. B **46**, 9128 (1992); M. Matsuda *et al.*, *ibid.*, **49**, 6958 (1994); K. Yamada *et al.*, Phys. Rev. Lett., **75**, 1526 (1995).
- [3] J. Rossat-Mignod *et al.*, Physica (Amsterdam) **185C**, 86 (1991).
- [4] J. M. Tranquada *et al.*, Phys. Rev. B **46**, 5561 (1992); B. J. Sternlieb *et al.*, *ibid.* **50**, 12915 (1994).
- [5] H. A. Mook *et al.*, Phys. Rev. Lett. **70**, 3490 (1993); Physica (Amsterdam) **213B**, 43 (1995).
- [6] H. F. Fong *et al.*, Phys. Rev. Lett. **75**, 316 (1995); Phys. Rev. B **54**, 6708 (1996).
- [7] P. Bourges *et al.*, Phys. Rev. B **53**, 876 (1996).
- [8] P. Dai *et al.*, Phys. Rev. Lett. **77**, 5425 (1996).
- [9] H. F. Fong *et al.*, Phys. Rev. Lett. **78**, 713 (1997).
- [10] J. P. Lu, Phys. Rev. Lett. **68**, 125 (1992).
- [11] Y. Zha *et al.*, Phys. Rev. B **47**, 9124 (1993).
- [12] Q. Si *et al.*, Phys. Rev. B **47**, 9055 (1993); P. B. Littlewood *et al.*, *ibid.* **48**, 487 (1993); T. Tanamoto *et al.*, J. Phys. Soc. Jpn. **63**, 2739 (1994).
- [13] R. E. Walsted *et al.*, Phys. Rev. Lett. **72**, 3610 (1994).
- [14] V. Barzykin *et al.*, Phys. Rev. B **50**, 16052 (1994).
- [15] Y. Zha *et al.*, Phys. Rev. B **54**, 7561 (1996).

- [16] J. M. Tranquada *et al.*, *Nature* **375**, 561 (1995); Phys. Rev. B **54**, 7489 (1996); Phys. Rev. Lett. **78**, 338 (1997).
- [17] J. Zaanen and O. Gunnarsson, Phys. Rev. B **40**, 7391 (1989); U. Löw *et al.*, Phys. Rev. Lett. **72**, 1918 (1994); C. Castellani *et al.*, *ibid.* **75**, 4650 (1995).
- [18] V. J. Emery and S. A. Kivelson, Physica C **209**, 597 (1993); *ibid.* **235**, 189 (1994); V. J. Emery *et al.*, unpublished (1997).
- [19] H. A. Mook and B. C. Chakoumakos, unpublished (1997).
- [20] R. M. Moon *et al.*, Phys. Rev. **181**, 920 (1969).
- [21] H. A. Mook *et al.*, Phys. Rev. Lett. **77**, 370 (1996).
- [22] The high energy transfer measurements at the ISIS pulsed spallation source [See, for example, S. M. Hayden *et al.*, Phys. Rev. B, **54**, R6905 (1996).] on the sample show that the optical modes appear first at  $60 \pm 5$  meV, thus it is sufficient to model the magnetic fluctuations with the acoustic modulation for the energy range probed in the present experiment.
- [23] Here we have adopted the notation of Ref. [4]. The expression  $\chi''(\omega) \propto \omega$  is valid for  $\omega \rightarrow 0$  [15] and we have extended it to give an estimate of the integration range.
- [24] In Ref. [8], we have observed a drop in magnetic signal at  $(\pi, \pi)$ . Unfortunately, the polarized constant-energy scan at 24 meV (see Fig. 2(b) of Ref. [8]) did not pick up the incommensurate feature described in this work due to limited intensity of the technique.

## FIGURES

FIG. 1. (a) Diagram of reciprocal space probed in the experiment. The dashed arrow indicates the scan direction with the integrated technique while the solid arrow represents the triple-axis measurements. (b) Calculated scattered intensity  $I(\mathbf{q}, \omega)$  as a function of energy transfer. The effective energy integration range is mostly from 10 to 30 meV. Note  $k_f$  is parallel to  $q_z$  in this technique. (c) Integrated measurements in which the data at 295 K are subtracted from 200 K, 150 K, 100 K, 65 K, and 15 K. The data are normalized to the same monitor count. The solid lines in the 100 K, 150 K, and 200 K data are fits to single Gaussians and linear backgrounds. The solid lines in the 15 and 65 K data are two Lorentzian-squared peaks on linear backgrounds which best fit the data.

FIG. 2. Triple-axis scans along  $(H, 3H, 1.7)$  at 24 meV for (a) 295 K, (b) 70 K, (c) 58 K, and (d) 50 K. Data at 295 K were collected with HB-1 while other scans were taken using HB-3. Since room temperature measurements at 42 meV [Fig. 3(c)] show no peak at  $(\pi, \pi)$ , the weak structures in (a) are most likely due to phonon and/or spurious processes. The horizontal bar shows the resolution along the scan direction and the vertical resolution is  $0.14 \text{ \AA}^{-1}$ . The positions of incommensuration at  $H \approx 0.48$  and  $0.53$  r.l.u. are indicated by the arrows. Solid lines in (b)-(d) are two Lorentzian-squared peaks on a linear background. The increased scattering at  $H > 0.6$  r.l.u. is due to phonons.

FIG. 3. Constant-energy scans along  $(H, 3H, 1.7)$  with energy transfer of 34 meV at (a) 75 K, and (b) 15 K. Identical scans at 42 meV at (c) 295 K ( $\bullet$ ), 75 K ( $\circ$ ), and (d) 15 K ( $\circ$ ). Inset ( $\bullet$ ) shows the temperature dependence of the scattering at  $(0.5, 1.5, -1.7)$  for  $\Delta E = 42$  meV where the arrow indicates  $T_c$ . The multi-phonon background in the 295 K data has been scaled to the value at 75 K for clarity. Solid lines are Gaussian fits to the data. The  $\mathbf{q}$  width of the resonance after deconvolving the resolution (horizontal bar) is  $0.23 \text{ \AA}^{-1}$ . A similar result is obtained at 42 meV.

FIG. 4. Difference spectra along  $(H, 3H, 1.7)$  between low temperature ( $< T_c$ ) and high temperature ( $\approx T_c + 12$  K) at (a) 24 meV, (b) 27 meV, (c) 34 meV, and (d) 42 meV. All data were taken with the same monitor units. To a very good approximation, the data can be regarded as the difference in susceptibility between 15 K and 75 K, *i.e.*,  $\chi''(15 \text{ K}) - \chi''(75 \text{ K})$ . Solid lines are guides to the eye. (e) Summary of triple-axis measurements. Open squares indicate incommensurate positions. Solid and open circles are the resonance and fluctuations at 42 meV, respectively. The error bars show the energy resolution and the intrinsic  $\mathbf{q}$  width (FWHM).

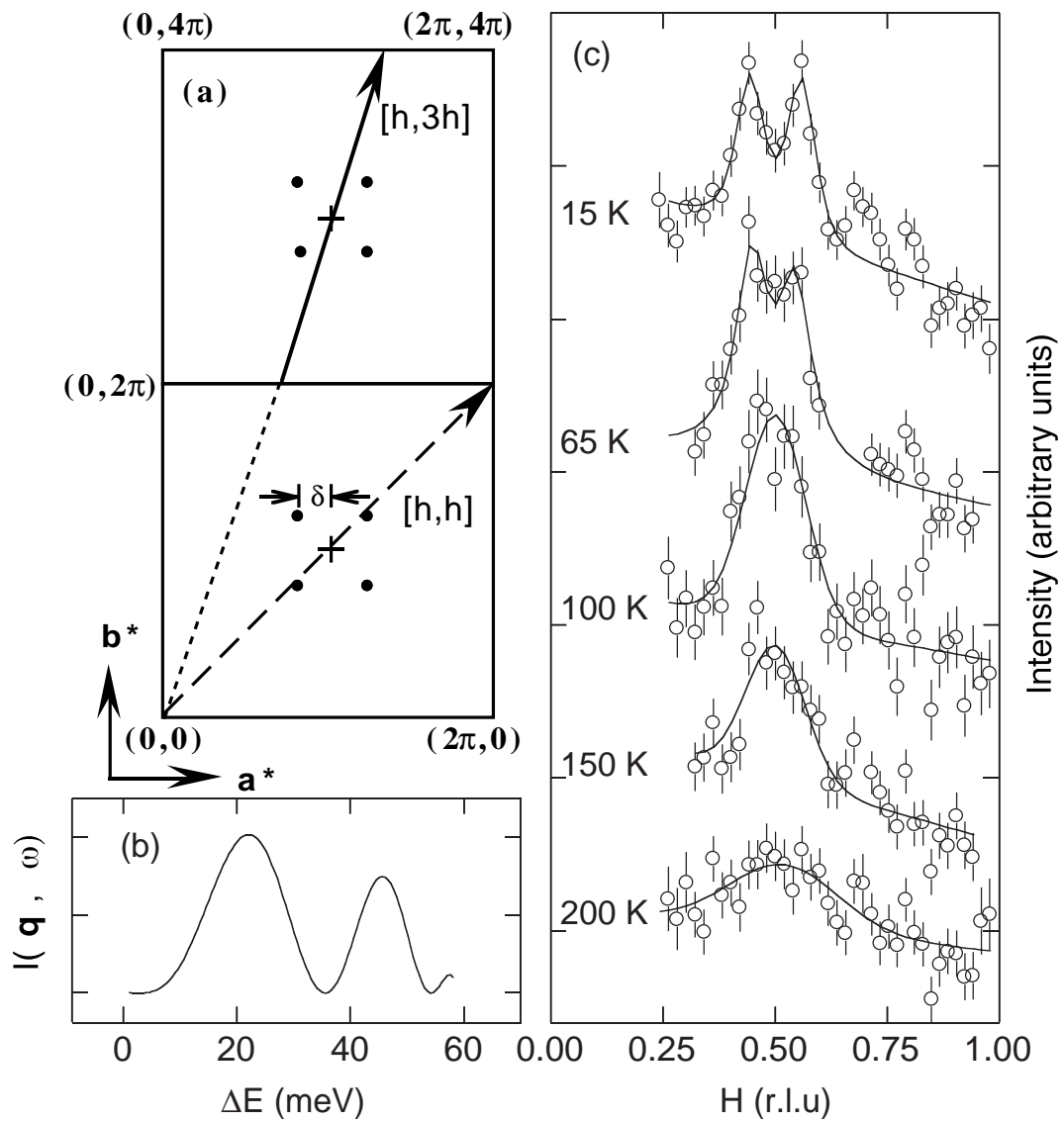


Figure 1  
P. Dai et al.

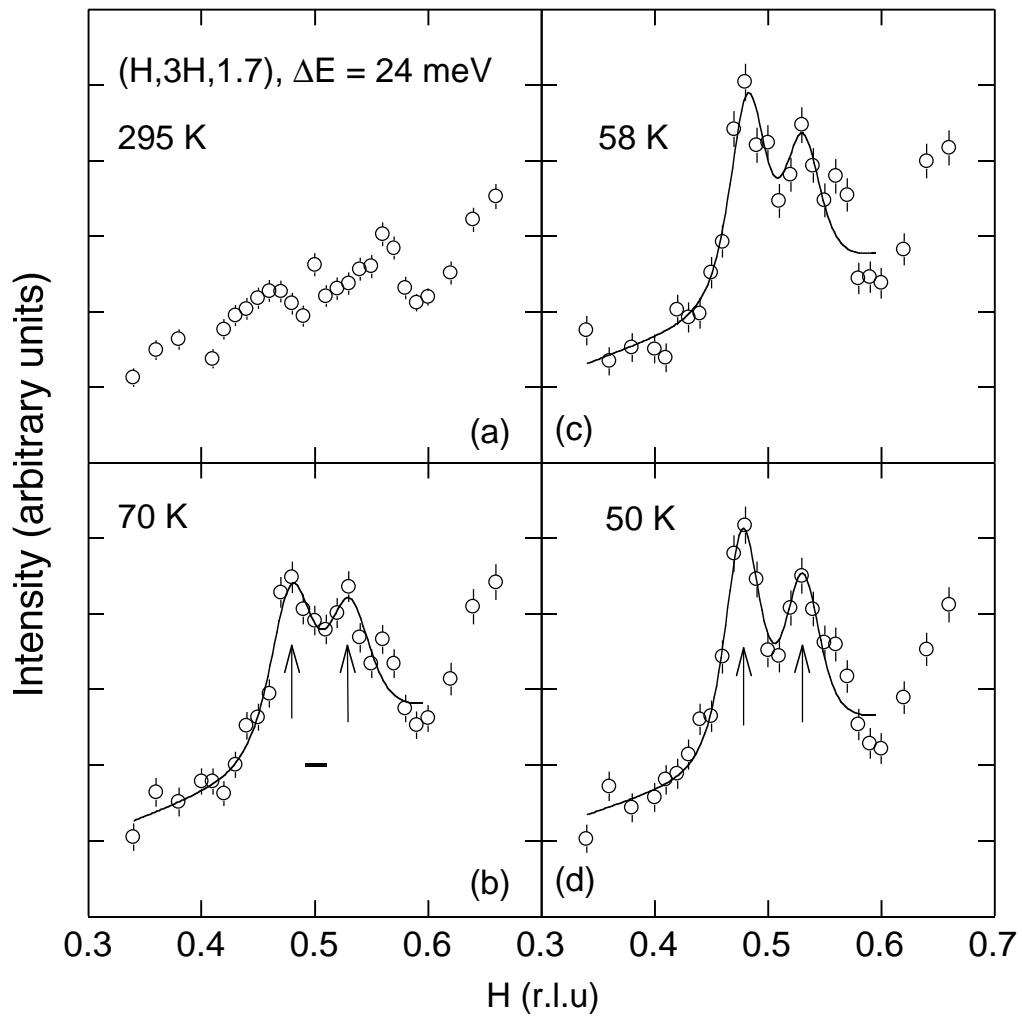


Figure 2  
P. Dai et al.

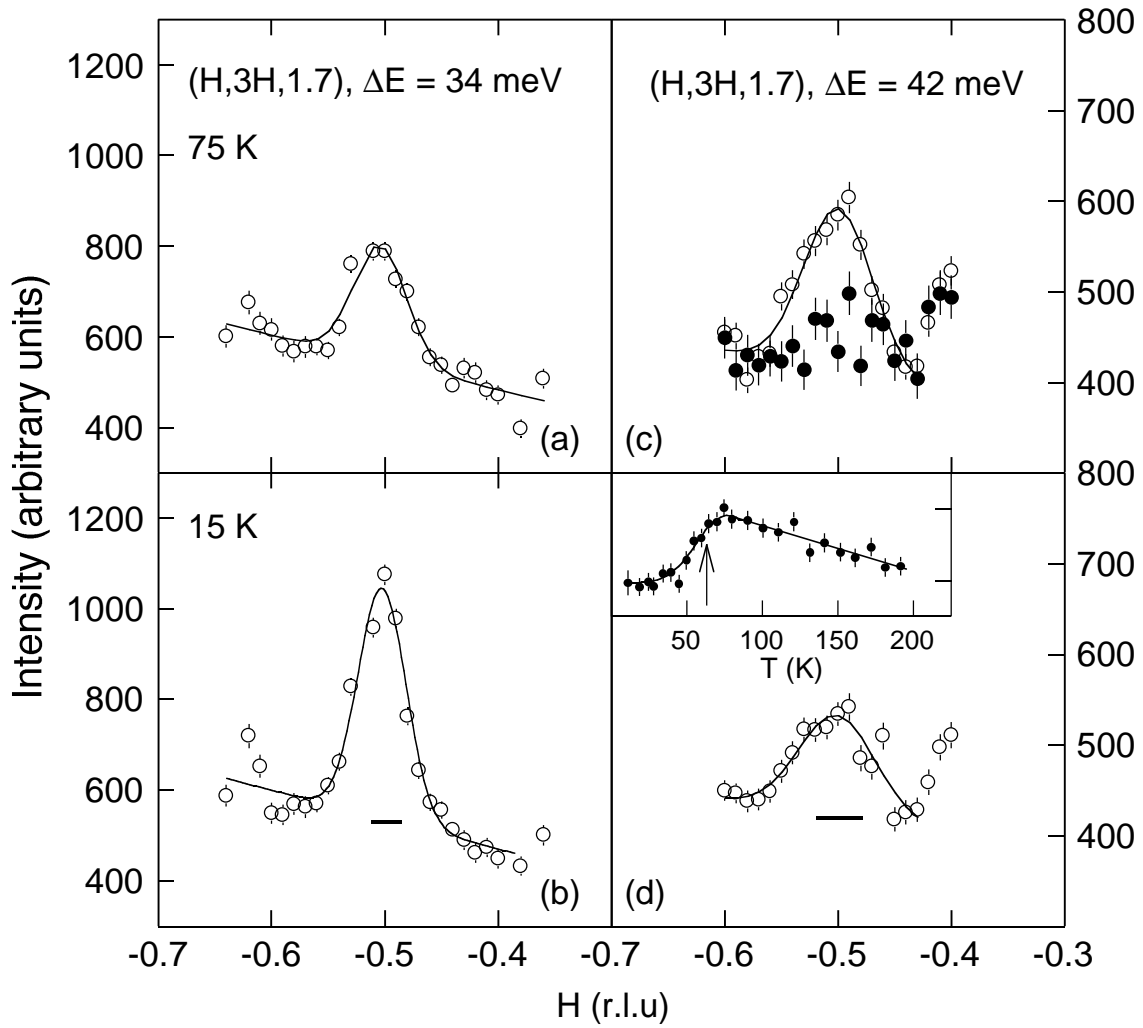


Figure 3  
P. Dai et al.

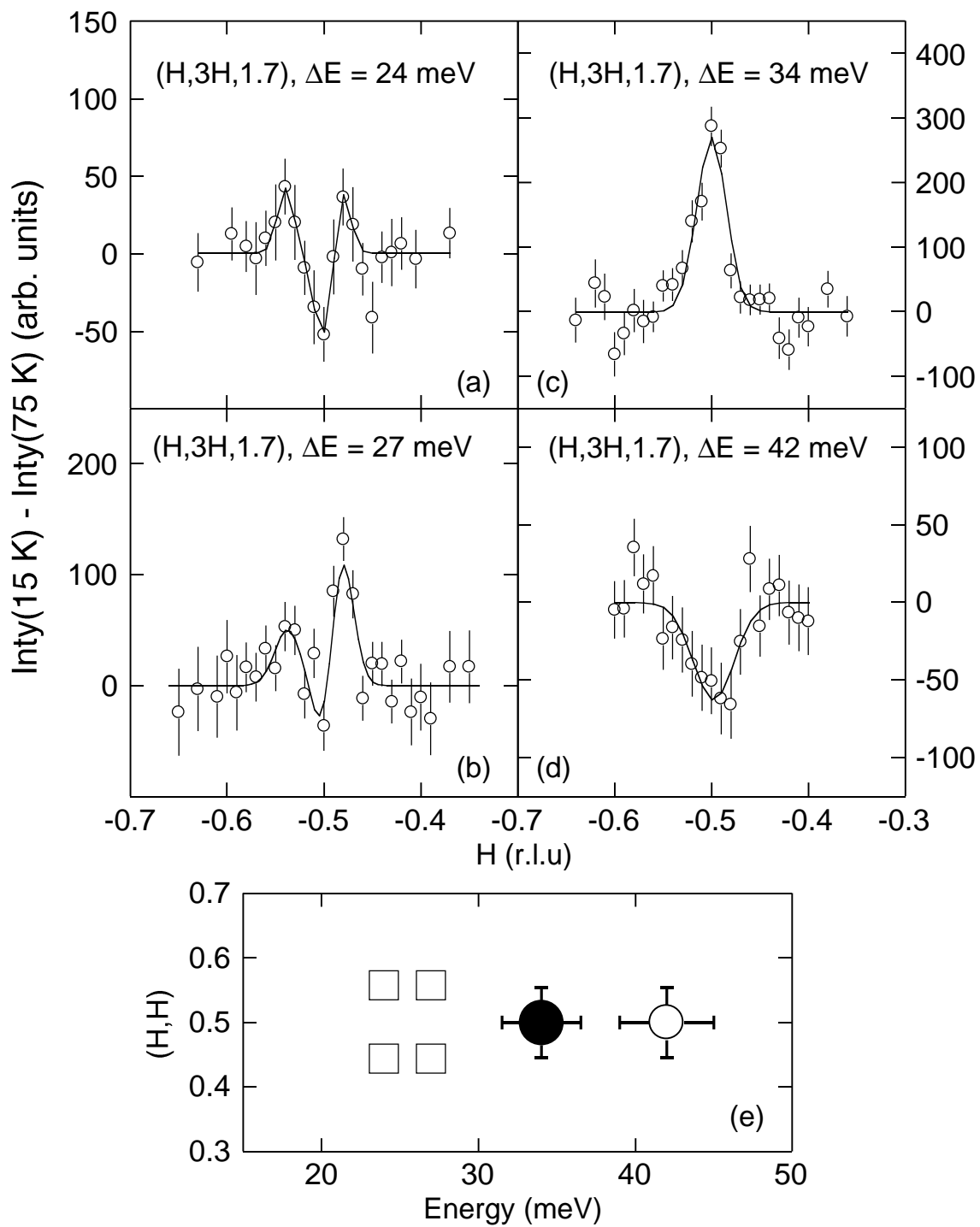


Figure 4  
P. Dai et al.